frontiers | Frontiers in Electronic Materials

ORIGINAL RESEARCH
published: 07 April 2022
doi: 10.3389/femat.2022.878308

# Effects of the Order Parameter Anisotropy on the Vortex Lattice in $UPt_3$

*K. E. Avers*[1,2†], *W. J. Gannon*[1,3], *A. W. D. Leishman*[4], *L. DeBeer-Schmitt*[5], *W. P. Halperin*[1] *and M. R. Eskildsen*[4*]

[1]Department of Physics and Astronomy, Northwestern University, Evanston, IL, United States, [2]Center for Applied Physics and Superconducting Technologies, Northwestern University, Evanston, IL, United States, [3]Department of Physics and Astronomy, University of Kentucky, Lexington, KY, United States, [4]Department of Physics, University of Notre Dame, Notre Dame, IN, United States, [5]Large Scale Structures Section, Neutron Scattering Division, Oak Ridge National Laboratory, Oak Ridge, TN, United States

OPEN ACCESS

**Edited by:**
Jeffrey W. Lynn,
National Institute of Standards and Technology (NIST), United States

**Reviewed by:**
Robert James Joynt,
University of Wisconsin-Madison, United States
Dong Qian,
Shanghai Jiao Tong University, China

***Correspondence:**
M. R. Eskildsen
eskildsen@nd.edu

**†Present address:**
K. E. Avers,
Department of Physics, University of Maryland, College Park, MD, United States

**Specialty section:**
This article was submitted to Superconducting Materials, a section of the journal Frontiers in Electronic Materials

**Received:** 17 February 2022
**Accepted:** 08 March 2022
**Published:** 07 April 2022

**Citation:**
Avers KE, Gannon WJ, Leishman AWD, DeBeer-Schmitt L, Halperin WP and Eskildsen MR (2022) Effects of the Order Parameter Anisotropy on the Vortex Lattice in $UPt_3$. Front. Electron. Mater. 2:878308. doi: 10.3389/femat.2022.878308

We have used small-angle neutron scattering to determine the vortex lattice phase diagram in the topological superconductor $UPt_3$ for the applied magnetic field along the crystalline *c*-axis. A triangular vortex lattice is observed throughout the superconducting state, but with an orientation relative to the hexagonal basal plane that changes with field and temperature. At low temperature, in the chiral B phase, the vortex lattice undergoes a non-monotonic rotation with increasing magnetic field. The rotation amplitude decreases with increasing temperature and vanishes before reaching the A phase. Within the A phase an abrupt ±15° vortex lattice rotation was previously reported by Huxley *et al.*, Nature **406**, 160-164 (2000). The complex phase diagram may be understood from competing effects of the superconducting order parameter, the symmetry breaking field, and the Fermi surface anisotropy. The low-temperature rotated phase, centered around 0.8 T, reported by Avers *et al.*, Nature Physics **16**, 531-535 (2020), can be attributed directly to the symmetry breaking field.

**Keywords: vortex lattice (superconductors), heavy fermion supercoductor, topological superconductor, $UPt_3$, small-angle neutron scattering**

## 1 INTRODUCTION

With three distinct superconducting phases $UPt_3$ has attracted significant attention (Joynt and Taillefer, 2002), but despite decades of experimental and theoretical studies the unconventional superconductivity in this material is still not fully understood. **Figure 2B** shows the $UPt_3$ phase diagram, indicting the extent of the superconducting A, B and C phases. The presence of two distinct zero-field superconducting transitions suggests that the order parameter belongs to one of the two-dimensional representations of the $D_{6h}$ point group (Hess et al., 1989). Here, *f*-wave pairing states with the $E_{2u}$ irreducible representation are the most likely (Sauls, 1994). In such a scenario the B phase breaks time reversal and mirror symmetries while the A and C phases are time-reversal symmetric. Experimental support comes from the *H-T* phase diagram (Shivaram et al., 1986; Adenwalla et al., 1990; Choi and Sauls, 1991; Sauls, 1994), and thermodynamic and transport studies (Taillefer et al., 1997; Graf et al., 2000). Broken time-reversal symmetry in the B phase is supported by phase-sensitive Josephson tunneling (Strand et al., 2009), the observation of polar Kerr rotation (Schemm et al., 2014), and a field history-dependent vortex lattice (VL) configuration (Avers et al., 2020). Finally, the linear temperature dependence of the London penetration depth is consistent with

a quadratic dispersion of the energy gap at the polar nodes structure, which is a characteristic of the $E_{2u}$ model (Signore et al., 1995; Schöttl et al., 1999; Gannon et al., 2015).

A key component in the understanding of superconductivity in $UPt_3$ is the presence of a symmetry breaking field (SBF) that couples to the $E_{2u}$ superconducting order parameter (Hayden et al., 1992). The SBF lifts the degeneracy of the multi-dimensional representation, splitting the zero-field transition and leading to the multiple superconducting phases (Sauls, 1994). However, the origin of the SBF is an outstanding issue, with possible candidates that include a quasi-static antiferromagnetic state that develops at 5 K above the superconducting transition (Aeppli et al., 1988a; Aeppli et al., 1988b; Hayden et al., 1992), a distortion of the hexagonal crystal structure (Walko et al., 2001), or prismatic plane stacking faults (Hong, 1999; Gannon et al., 2012).

Vortices provide a highly sensitive probe of the host superconductor. This includes anisotropies in the screening current plane perpendicular to the applied magnetic field which affect the VL symmetry and orientation. Such anisotropies may arise from the Fermi surface (Kogan, 1981; Kogan et al., 1997), and nodes in or distortions of the superconducting gap (Huxley et al., 2000; Avers et al., 2020). As an example one can consider the "simple" superconductor niobium that displays a rich VL phase diagram when the applied field is along the (100) crystalline direction and the Fermi surface anisotropy is incommensurate with an equilateral triangular VL (Laver et al., 2006; Laver et al., 2009; Mühlbauer et al., 2009). Even in materials with a hexagonal crystal structure VL rotations may occur due to competing anisotropies, as observed in $MgB_2$ when the applied field is perpendicular to the basal plane (Cubitt et al., 2003; Das et al., 2012).

We have used small-angle neutron scattering (SANS) to determine the VL phase diagram in $UPt_3$. This extends our previous studies at low temperature, where the VL was found to undergo a field-driven, non-monotonic rotation transition (Avers et al., 2020). We discuss how the VL phase diagram and the existence of the VL rotation transition can be directly attributed to the SBF.

## 2 EXPERIMENTAL DETAILS

Small-angle neutron scattering studies of the VL are possible due to the periodic field modulation from the vortices (Mühlbauer et al., 2019). The scattered intensity depends strongly on the superconducting penetration depth, and for $UPt_3$ with a large in-plane $\lambda_{ab} \sim 680$ nm (Gannon et al., 2015) necessitates a large sample volume. For this work we used a high-quality single crystal (ZR11), combined with previously published results obtained on a separate sample (ZR8) (Avers et al., 2020). Properties of both single crystals are listed in **Table 1**, determined from resistive measurements performed on smaller samples cut from the main crystals. Here, RRR is the residual resistivity ratio, $T_c$ is the superconducting transition temperature and $\Delta T_c$ is the width of the transition. For the SANS measurements each long, rod-like crystal was cut into two pieces, co-aligned and fixed with silver epoxy (EPOTEK E4110) to a copper cold finger. The sample assembly was mounted onto the mixing chamber of a dilution refrigerator and placed inside a superconducting magnet, oriented with the crystalline **a** axis vertical and the **c** axis horizontally along the magnetic field and the neutron beam. The neutron beam was masked off to illuminate a $7 \times 11$ mm$^2$ area.

**TABLE 1 |** Properties of the two $UPt_3$ single crystals used for the SANS experiments.

| Sample | Mass (g) | RRR | $T_c$ (mK) | $\Delta T_c$ (mK) |
|---|---|---|---|---|
| ZR8 | 15 | >600 | 560 ± 2 | 10 |
| ZR11 | 9 | >900 | 557 ± 2 | 5 |

The SANS experiment was performed at the GP-SANS beam line at the High Flux Isotope Reactor at Oak Ridge National Laboratory (Heller et al., 2018). All measurements were carried out in a "rocked on" configuration, satisfying the Bragg condition for VL peaks at the top of the two-dimensional position sensitive detector, as seen in **Figure 1**. Background measurements, obtained either in zero field or above $H_{c2}$, were subtracted from both the field reduction and field reversal data.

Measurements were performed at temperatures between 100 and 300 mK and fields between 0.4 and 1.2 T. Prior to the SANS measurements the field was reduced from above the B-C phase transition at base temperature. The sample was then heated to the measurement temperature and a damped field oscillation with an initial amplitude of 20 mT was applied to obtain a well ordered VL with a homogeneous vortex density (Avers et al., 2020). Furthermore, a 5 mT field oscillation was applied approximately every 60 s during the SANS measurements, in order to counteract VL disordering due to neutron induced fission of $^{235}$U (Avers et al., 2021).

## 3 RESULTS

**Figure 1** shows VL diffraction patterns obtained in an applied field of 0.6 T and temperature between 100 and 300 mK. As previously reported, the VL in $UPt_3$ has a triangular symmetry but is in general not oriented along a high symmetry direction of the hexagonal crystalline basal lattice ($\boldsymbol{a}$ or $\boldsymbol{a}^*$) (Avers et al., 2020). This causes the VL to break up into clockwise and counterclockwise rotated domains, and gives rise to the Bragg peak splitting in **Figures 1A,B**. With increasing temperature the splitting decreases, and the two peaks eventually merge as seen in **Figure 1C**.

To quantify the VL rotation we define the peak splitting angle ($\omega$) shown in **Figure 1A**, determined from two-Gaussian fits to the diffraction pattern intensity. Specific details of the fitting will be discussed in more detail later. The temperature dependence of $\omega$ is summarized in **Figure 2A** for all the magnetic fields measured, together with results from our previous SANS studies obtained at base temperature (Avers et al., 2020).

At all fields the temperature dependence of $\omega$ appears to be linear within the measurement error, and extrapolate to zero well

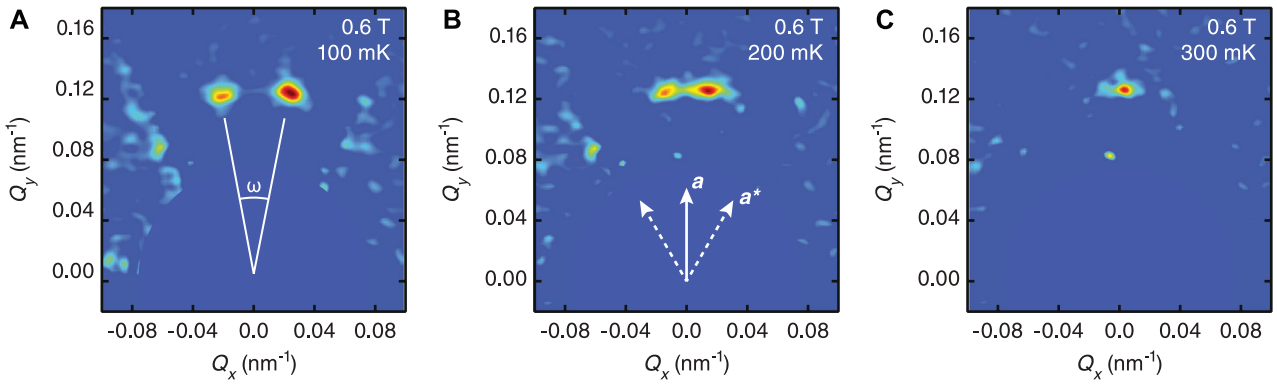


**FIGURE 1 |** SANS VL diffraction patterns obtained at $H = 0.6$ T and $T = 100$ mK **(A)**, 200 mK **(B)** and 300 mK **(C)**. The Bragg peak splitting ($\omega$) is indicated in **(A)** and crystallographic directions within the scattering plane in **(B)**. Only peaks at the top of the detector were imaged. Zero field background scattering is subtracted, and the detector center near $Q = 0$ is masked off.

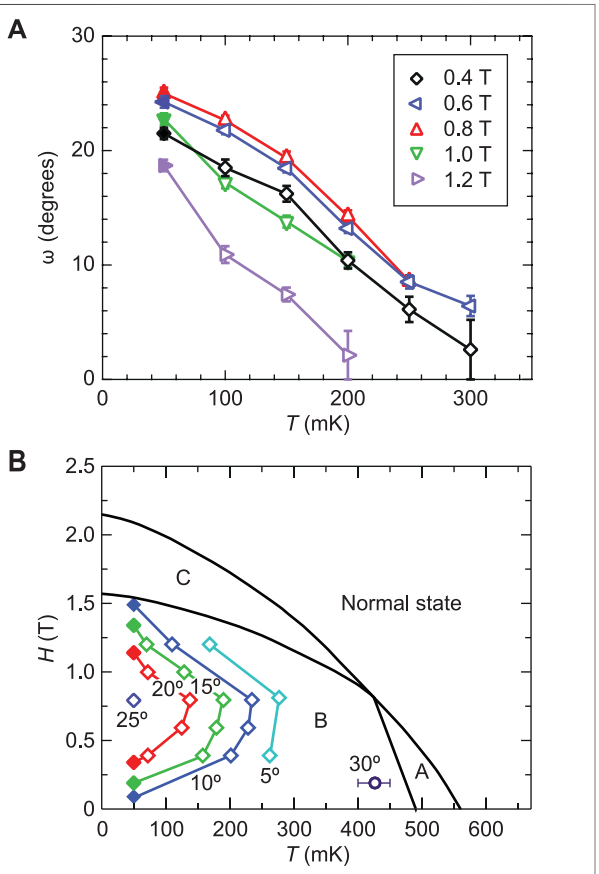


**FIGURE 2 |** Vortex lattice rotation. **(A)** VL peak splitting vs. temperature for different magnetic fields. The data at 50 mK (solid symbols) was previously obtained on the ZR8 crystal (Avers et al., 2020). Error bars represent one standard deviation. **(B)** Constant $\omega$ contours superimposed on the $UPt_3$ phase diagram. Values are obtained from the data in **(A)** by interpolation (open diamonds) and from the 50 mK field dependence in Ref. 11 (solid diamonds). The 30° data point (open circle) is from previous work by (Huxley et al., 2000).

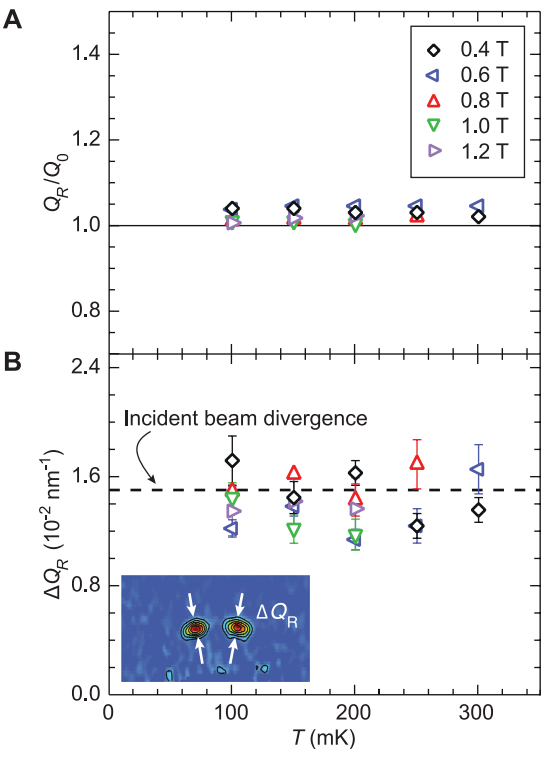


**FIGURE 3 |** Vortex lattice density. **(A)** Scattering vector magnitude normalized to the value expected for a triangular VL. **(B)** Radial width of the VL Bragg peaks (FWHM) compared to the incident beam divergence (dashed line). The inset indicates $\Delta Q_R$ within the detector plane.

below the A-B phase transition. The larger error bars at higher temperature is due to an increasing penetration depth and the resulting decrease in the scattered intensity (Gannon et al., 2015). **Figure 2B** shows $\omega$ equicontours superimposed on the $UPt_3$ $H$-$T$ phase diagram. The nonmonotonic behavior, previously reported

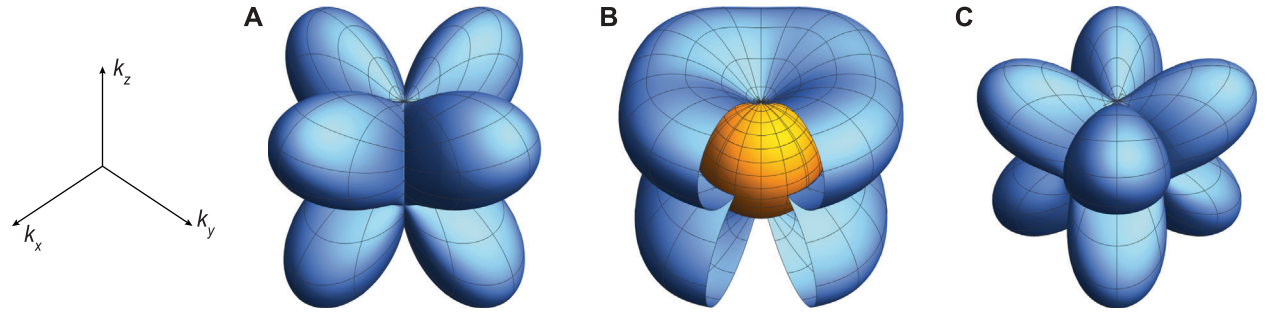


**FIGURE 4 |** Order parameter in the **(A)** A phase ($\eta_1 \neq 0$, $\eta_2 = 0$), **(B)** B phase distorted by the SBF ($\eta_1 = \eta_2 = 1$, $\epsilon = 0.1$), and **(C)** C phase ($\eta_1 = 0$, $\eta_2 \neq 0$).

at base temperature (Avers et al., 2020), is clearly observed at higher temperatures, although with a decreasing amplitude. Furthermore, the splitting extrapolates to zero in the zero field limit, and also decreases upon approaching the B-C phase transition. However, once in the C phase the splitting remains at a fixed value of ~ 8° (Avers et al., 2020). At all temperatures the maximal VL rotation is observed at 0.8 T. Also indicated in **Figure 2B** is the approximate temperature at 0.19 T at which $\omega$ reaches 30° in the vicinity of the A phase, reported by (Huxley et al., 2000).

Ensuring a reliable determination of $\omega$ requires a careful approach to the fitting. At all fields and temperatures the radial position ($Q_R$) as well as the radial ($\Delta Q_R$) and azimuthal ($\Delta\theta$) widths were constrained to be the same for both of the split peaks. Furthermore, the azimuthal width at each field was determined from fits at low temperature where the peaks are clearly separated, and then kept fixed at the higher temperature where they begin to overlap. To justify this approach, we note that when the peaks are clearly separated, $\Delta\theta$ does not exhibit any systematic temperature dependence. The azimuthal width does show a field dependence, however, with $\Delta\theta$ decreasing from ~ 11.5° FWHM at 0.4 T to ~ 6.5° FWHM at 1.2 T.

The VL density is reflected in $Q_R$ and $\Delta Q_R$, shown in **Figure 3**. The magnitude of the scattering vector in **Figure 3A** agrees to within a few percent with $Q_0 = 2\pi(\sqrt{3}/2)^{1/4}\sqrt{B/\Phi_0}$ expected for a triangular VL and assuming that the magnetic induction ($B$) is equal to the applied magnetic field. Here $\Phi_0 = h/2e = 2069$ T nm$^2$ is the flux quantum. The small deviation between $Q_R$ and $Q_0$ is slightly greater at low fields consistent with earlier work (Avers et al., 2020), but notably independent of temperature. Similarly, there is no systematic temperature or field dependence in the radial width in **Figure 3B**. However, the values are systematically at or below the divergence of the incident beam, indicating a highly ordered VL which leads to a diffracted neutron beam that is, more collimated than the incident one.

## 4 DISCUSSION

The complex VL phase diagram in **Figure 2B** reflects the presence of multiple competing effects. In the following we discuss how, at the qualitative level, this phase diagram arises from the interplay between the SBF and the nodal configuration of the superconducting energy gap for the A and C phases. A more detailed treatment of the VL structure and orientation within the A phase was provided by Champel and Mineev (Champel and Mineev, 2001). First, however, we note that $\omega \to 0$ in the limit $T = H = 0$. For large vortex separations the order parameter has a vanishing effect on the VL, and the orientation with Bragg peaks along the **a** axis must be due to the Fermi surface anisotropy (Huxley et al., 2000; Champel and Mineev, 2001).

In momentum space the two-component $E_{2u}$ order parameter proposed for $UPt_3$ is given by (Sauls, 1994)

$$\Delta(\mathbf{k}) = \left(\eta_1\left(k_x^2 - k_y^2\right) \pm 2i\,\eta_2\,(1-\epsilon)\,k_x\,k_y\right)k_z. \tag{1}$$

Here, $\eta_1$ and $\eta_2$ are real amplitudes which depend on temperature and magnetic field and $\epsilon$ is due to the SBF. The A and C phases correspond to a vanishing of $\eta_2$ and $\eta_1$ respectively. The magnitude of the SBF determines the zero-field split in the superconducting transition ($\Delta T_{AB}$) and thus the width of the A phase. Experimentally, $\Delta T_{AB} \approx 55$ mK which yields $\epsilon \propto \frac{\Delta T_{AB}}{T_c} \approx 0.1$ (Sauls, 1994). Within the B phase both components of the order parameter are non-zero, although with different amplitudes. Due to the SBF this imbalance persists even in the low-temperature, low-field limit where both $\eta_2$ and $\eta_1$ approach unity (Sauls, 1994). The order parameter structure is illustrated in **Figure 4**.

Within the A phase SANS studies by Huxley *et al.* found a VL with domains rotated by ± 15° relative to the **a** axis ($\omega = 30°$) (Huxley et al., 2000). The VL rotation was attributed to a competition between the sixfold Fermi surface anisotropy and the fourfold anisotropy of the nodal structure in the A phase (Huxley et al., 2000; Champel and Mineev, 2001). Notably, the rotation persists into the B phase as indicated in **Figure 2B**. This is not surprising since the $\eta_1/\eta_2 \to \infty$ upon approaching the A phase from low temperature, where the B phase order parameter therefore exhibit a substantial fourfold anisotropy. However, as $\eta_2$ increases with decreasing temperature this ratio quickly decreases, causing an abrupt transition to $\omega = 0$ around 425 mK (Huxley et al., 2000).

Due to the SBF the order parameter in the B phase preserves a degree of fourfold anisotropy, as shown in **Figure 4**. This anisotropy is oriented in a manner similar to the A phase, with an effect on the vortex-vortex interactions which will

increase with increasing field (vortex density). The influence of the SBF anisotropy will increase further at low temperature as the superfluid density increases (Gannon et al., 2015), even if $\epsilon$ remains fixed. This explains the initial increase of $\omega$ with field at low temperatures, with an amplitude (0.8 T) that extrapolates to a value close to 30° for $T \rightarrow 0$.

As the field is increased further and approaches the BC phase transition, $\eta_1$ decreases and finally vanish. The C phase order parameter is rotated by 45° about $k_z$ with respect to the B phase, as shown in **Figure 4**. This will favor a VL oriented along the **a** axis, i.e., the same as the Fermi surface anisotropy, and explains the non-monotonic VL rotation as a function of field. Once $\eta_1$ has fully vanished no further VL rotation is expected, in agreement with the observed field-independence of $\omega \approx 8°$ in the C phase (Avers et al., 2020).

## 5 CONCLUSION

In summary, the rotated VL phase at low temperatures and intermediate fields in **Figure 2B** can be directly attributed to the SBF. To our knowledge this is the first observation of such an effect at the microscopic level, and may provide further constraints on the nature of both the SBF and the order parameter in $UPt_3$. A quantitative understanding of $\omega(T, H)$ will require a detailed theoretical analysis, taking into account the field and temperature dependence of the superfluid density as well as the complex Fermi surface of $UPt_3$. Here, the finite value of $\omega$ in the C phase is somewhat surprising and not obviously consistent with the order parameter in **Eq. 1**.

## DATA AVAILABILITY STATEMENT

The raw data supporting the conclusion of this article will be made available by the authors, without undue reservation.

## AUTHOR CONTRIBUTIONS

KA, WH, and ME conceived of the experiment. WG and KA grew and annealed the crystals. KA, AL, and ME performed the SANS experiments with assistance from LD-S. KA, WH, and ME wrote the paper with input from all authors.

## FUNDING

This work was supported by the Northwestern-Fermilab Center for Applied Physics and Superconducting Technologies (KA) and by the U.S. Department of Energy, Office of Basic Energy Sciences, under Awards No. DE-SC0005051 (ME: University of Notre Dame; neutron scattering) and DE-FG02-05ER46248 (WH: Northwestern University; crystal growth and neutron scattering). A portion of this research used resources at the High Flux Isotope Reactor, a DOE Office of Science User Facility operated by the Oak Ridge National Laboratory.

## ACKNOWLEDGMENTS

We are grateful to J. A. Sauls for numerous discussions and to V. P. Mineev for valuable feed-back.

## REFERENCES

Adenwalla, S., Lin, S. W., Ran, Q. Z., Zhao, Z., Ketterson, J. B., Sauls, J. A., et al. (1990). Phase Diagram ofUPt3from Ultrasonic Velocity Measurements. *Phys. Rev. Lett.* 65, 2298–2301. doi:10.1103/physrevlett.65.2298

Aeppli, G., Bucher, E., Broholm, C., Kjems, J. K., Baumann, J., and Hufnagl, J. (1988). Magnetic Order and Fluctuations in superconductingUPt3. *Phys. Rev. Lett.* 60, 615–618. doi:10.1103/physrevlett.60.615

Aeppli, G., Bucher, E., Goldman, A. I., Shirane, G., Broholm, C., and Kjems, J. K. (1988). Magnetic Correlations in UPt3 and U1−xThxPt3. *J. Magnetism Magn. Mater.* 76-77, 385–390. doi:10.1016/0304-8853(88)90430-1

Avers, K. E., Gannon, W. J., Kuhn, S. J., Halperin, W. P., Sauls, J. A., DeBeer-Schmitt, L., et al. (2020). Broken Time-Reversal Symmetry in the Topological Superconductor UPt3. *Nat. Phys.* 16, 531–535. doi:10.1038/s41567-020-0822-z

Avers, K. E., Kuhn, S. J., Leishman, A. W. D., Gannon, W. J., DeBeer-Schmitt, L., Dewhurst, C. D., et al. (2021). Reversible Ordering and Disordering of the Vortex Lattice in $UPt_3$. arXiv:2103.09843.

Champel, T., and Mineev, V. P. (2001). Theory of Equilibrium Flux Lattice inUPt3under Magnetic Field Parallel to Hexagonal Crystal Axis. *Phys. Rev. Lett.* 86, 4903–4906. doi:10.1103/physrevlett.86.4903

Choi, C., and Sauls, J. (1991). Identification of Odd-Parity Superconductivity in UPt_{3} from Paramagnetic Effects on the Upper Critical Field. *Phys. Rev. Lett.* 66, 484–487. doi:10.1103/physrevlett.66.484

Cubitt, R., Eskildsen, M. R., Dewhurst, C. D., Jun, J., Kazakov, S. M., and Karpinski, J. (2003). Effects of Two-Band Superconductivity on the Flux-Line Lattice in Magnesium Diboride. *Phys. Rev. Lett.* 91, 047002. doi:10.1103/physrevlett.91.047002

Das, P., Rastovski, C., O'Brien, T. R., Schlesinger, K. J., Dewhurst, C. D., DeBeer-Schmitt, L., et al. (2012). Observation of Well-Ordered Metastable Vortex Lattice Phases in SuperconductingMgB2Using Small-Angle Neutron Scattering. *Phys. Rev. Lett.* 108, 167001. doi:10.1103/physrevlett.108.167001

Gannon, W. J., Halperin, W. P., Rastovski, C., Eskildsen, M. R., Dai, P., and Stunault, A. (2012). Magnetization in the Superconducting State of UPt3from Polarized Neutron Diffraction. *Phys. Rev. B* 86, 104510. doi:10.1103/physrevb.86.104510

Gannon, W. J., Halperin, W. P., Rastovski, C., Schlesinger, K. J., Hlevyack, J., Eskildsen, M. R., et al. (2015). Nodal gap Structure and Order Parameter Symmetry of the Unconventional Superconductor UPt3. *New J. Phys.* 17, 023041. doi:10.1088/1367-2630/17/2/023041

Graf, M. J., Yip, S.-K., and Sauls, J. A. (2000). Identification of the Orbital Pairing Symmetry inUPt3. *Phys. Rev. B* 62, 14393–14402. doi:10.1103/physrevb.62.14393

Hayden, S. M., Taillefer, L., Vettier, C., and Flouquet, J. (1992). Antiferromagnetic Order inUPt3under Pressure: Evidence for a Direct Coupling to Superconductivity. *Phys. Rev. B* 46, 8675–8678. doi:10.1103/physrevb.46.8675

Heller, W. T., Cuneo, M., Debeer-Schmitt, L., Do, C., He, L., Heroux, L., et al. (2018). The Suite of Small-Angle Neutron Scattering Instruments at Oak Ridge National Laboratory. *J. Appl. Cryst.* 51, 242–248. doi:10.1107/s1600576718001231

Hess, D. W., Tokuyasu, T. A., and Sauls, J. A. (1989). Broken Symmetry in an Unconventional Superconductor: a Model for the Double Transition in UPt3. *J. Phys. Condens. Matter* 1, 8135–8145. doi:10.1088/0953-8984/1/43/014

Hong, J.-I. (1999). *Strucure-Property Relationships for a Heavy Fermion Superconductor $UPt_3$*. Evanston, IL: Northwestern University. PhD.

Huxley, A., Rodière, P., Paul, D. M., van Dijk, N., Cubitt, R., and Flouquet, J. (2000). Realignment of the Flux-Line Lattice by a Change in the Symmetry of Superconductivity in UPt3. *Nature* 406, 160–164. doi:10.1038/35018020

Joynt, R., and Taillefer, L. (2002). The Superconducting Phases ofUPt3. *Rev. Mod. Phys.* 74, 235–294. doi:10.1103/revmodphys.74.235

Kogan, V. G., Bullock, M., Harmon, B., Miranovic-acute, P., Dobrosavljevic-acute-Grujic-acute, L., Gammel, P. L., et al. (1997). Vortex Lattice Transitions in Borocarbides. *Phys. Rev. B* 55, R8693–R8696. doi:10.1103/physrevb.55.r8693

Kogan, V. G. (1981). London Approach to Anisotropic Type-II Superconductors. *Phys. Rev. B* 24, 1572–1575. doi:10.1103/physrevb.24.1572

Laver, M., Bowell, C. J., Forgan, E. M., Abrahamsen, A. B., Fort, D., Dewhurst, C. D., et al. (2009). Structure and Degeneracy of Vortex Lattice Domains in Pure Superconducting Niobium: A Small-Angle Neutron Scattering Study. *Phys. Rev. B* 79, 014518. doi:10.1103/physrevb.79.014518

Laver, M., Forgan, E. M., Brown, S. P., Charalambous, D., Fort, D., Bowell, C., et al. (2006). Spontaneous Symmetry-Breaking Vortex Lattice Transitions in Pure Niobium. *Phys. Rev. Lett.* 96, 167002. doi:10.1103/physrevlett.96.167002

Mühlbauer, S., Honecker, D., Périgo, E. A., Bergner, F., Disch, S., Heinemann, A., et al. (2019). Magnetic Small-Angle Neutron Scattering. *Rev. Mod. Phys.* 91, 015004. doi:10.1103/revmodphys.91.015004

Mühlbauer, S., Pfleiderer, C., Böni, P., Laver, M., Forgan, E. M., Fort, D., et al. (2009). Morphology of the Superconducting Vortex Lattice in Ultrapure Niobium. *Phys. Rev. Lett.* 102, 136408. doi:10.1103/physrevlett.102.136408

Sauls, J. A. (1994). The Order Parameter for the Superconducting Phases of UPt3. *Adv. Phys.* 43, 113–141. doi:10.1080/00018739400101475

Schemm, E. R., Gannon, W. J., Wishne, C. M., Halperin, W. P., and Kapitulnik, A. (2014). Observation of Broken Time-Reversal Symmetry in the Heavy-Fermion Superconductor UPt 3. *Science* 345, 190–193. doi:10.1126/science.1248552

Schöttl, S., Schuberth, E. A., Flachbart, K., Kycia, J. B., Hong, J. I., Seidman, D. N., et al. (1999). Anisotropic Dc Magnetization of SuperconductingUPt3and Antiferromagnetic Ordering below 20 mK. *Phys. Rev. Lett.* 82, 2378–2381. doi:10.1103/physrevlett.82.2378

Shivaram, B. S., Rosenbaum, T. F., and Hinks, D. G. (1986). Unusual Angular and Temperature Dependence of the Upper Critical Field in UPt3. *Phys. Rev. Lett.* 57, 1259–1262. doi:10.1103/physrevlett.57.1259

Signore, P. J. C., Andraka, B., Meisel, M. W., Brown, S. E., Fisk, Z., Giorgi, A. L., et al. (1995). Inductive Measurements ofUPt3in the Superconducting State. *Phys. Rev. B* 52, 4446–4461. doi:10.1103/physrevb.52.4446

Strand, J. D., Van Harlingen, D. J., Kycia, J. B., and Halperin, W. P. (2009). Evidence for Complex Superconducting Order Parameter Symmetry in the Low-Temperature Phase ofUPt3from Josephson Interferometry. *Phys. Rev. Lett.* 103, 197002. doi:10.1103/physrevlett.103.197002

Taillefer, L., Ellman, B., Lussier, B., and Poirier, M. (1997). On the gap Structure of UPt3: Phases A and B. *Physica B: Condensed Matter* 230-232, 327–331. doi:10.1016/s0921-4526(96)00706-5

Walko, D. A., Hong, J. I., Rao, T. V. C., Wawrzak, Z., Seidman, D. N., Halperin, W. P., et al. (2001). Crystal Structure Assignment for the Heavy-Fermion Superconductor $UPt_3$. *Phys. Rev. B* 63, 054522. doi:10.1103/physrevb.63.054522

**Conflict of Interest:** The authors declare that the research was conducted in the absence of any commercial or financial relationships that could be construed as a potential conflict of interest.

**Publisher's Note:** All claims expressed in this article are solely those of the authors and do not necessarily represent those of their affiliated organizations, or those of the publisher, the editors and the reviewers. Any product that may be evaluated in this article, or claim that may be made by its manufacturer, is not guaranteed or endorsed by the publisher.